J. Fluid Mech. (1993), *vol.* 251, *pp.* 79–107

The formation of toroidal bubbles upon the collapse of transient cavities

By J. P. BEST
Materials Research Laboratory (MRL) – DSTO, PO Box 50, Ascot Vale, Victoria, 3032, Australia

(Received 12 June 1991 and in revised form 5 September 1992)

A spectacular feature of transient cavity collapse in the neighbourhood of a rigid boundary is the formation of a high-speed liquid jet that threads the bubble and ultimately impacts upon the side of the bubble nearest to the boundary. The bubble then evolves into some toroidal form, the flow domain being doubly connected. In this work, the motion of the toroidal bubble is computed by connecting the jet tip to the side of the bubble upon which it impacts. This connection is via a cut introduced into the flow domain and across which the potential is discontinuous, the value of this discontinuity being equal to the circulation in the flow. A boundary integral algorithm is developed to account for this geometry and some example computations are presented. Consideration of the pressure field in the fluid has implications for possible damage mechanisms to structures due to nearby cavity collapse.

1. Introduction

In their paper on cavitation, Benjamin & Ellis (1966) postulate that upon the collapse of a cavitation bubble in the neighbourhood of a rigid boundary, the bubble evolves into toroidal form, with an attached vortex ring. The circulation in the flow arises from the change in the flow topology from a singly connected to a doubly connected domain. As noted by these workers, the existence of the circulation in the flow field is necessary to conserve the Kelvin impulse. The theoretical discussions of Benjamin & Ellis (1966) were based on the experimental evidence embodied in high-speed photographic records of cavity collapse near to rigid boundaries. Owing to the greater mobility of the flow away from the boundary the collapse of the surface there proceeds at a greater speed than elsewhere, causing a jet to form and thread the bubble, ultimately impacting upon the far side of the bubble, nearest the boundary.

The formation of vortex ring bubbles has also been postulated upon the collapse of the bubble produced by an underwater explosion. The fluid dynamics of this phenomenon is very similar in character to that of the cavitation bubble. During early research into underwater explosions it was found that, based on computations assuming a spherical bubble, the apparent loss of energy per bubble oscillation could not be accounted for by the expected loss mechanisms of acoustic radiation, heat transfer and turbulence. This led to the postulate that the bubble evolves after the first collapse into a vortex ring bubble, with the quantity of kinetic energy bound in the vortex motion seeming to account for the apparent losses. For a discussion of this problem the reader is referred to the review by Holt (1977).

Numerical investigations of this jetting phenomenon have been undertaken and generally assume the irrotational flow of an incompressible and inviscid fluid. The first study of significance was that of Plesset & Chapman (1971) who employed a particle-

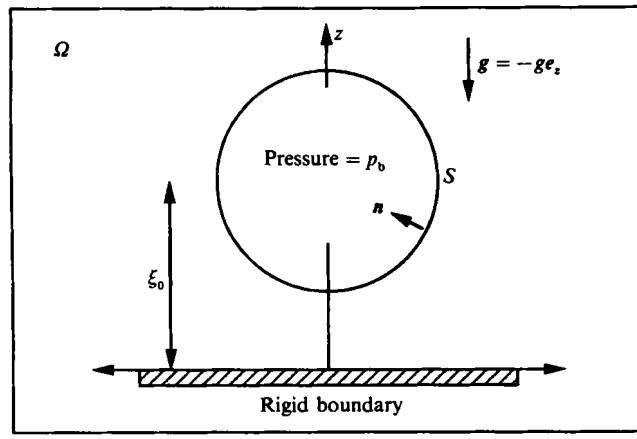

FIGURE 1. The geometry used to consider axisymmetric bubble motion in the neighbourhood of a rigid boundary.

in-cell technique to compute the collapse of an initially spherical bubble in the neighbourhood of a rigid boundary. This method was successful in predicting the formation and development of the jet up until the time that it impacts upon the far side of the bubble. Since this investigation, the boundary integral method has proved to be a successful technique for computing bubble motion (Guerri, Lucca & Prosperetti 1981; Blake, Taib & Doherty 1986, 1987); however, to date these calculations may only proceed up until the time that the jet impinges upon the far side of the bubble. We further remark that this method has recently been utilized to compute the motion of constant-volume vortex ring bubbles (Lundgren & Mansour 1991).

The fluid dynamics of the jet impact is complex, with compressibility, viscosity and surface tension expected to play a role. The magnitude of their contributions is expected to vary in different physical regimes, and we give this matter some consideration later in this paper in the light of both our numerical results and recent experimental observations. The aim of this study is to neglect such complicating factors and seek a solution of Laplace's equation in the doubly connected geometry that evolves from the solution in the singly connected domain, that describes the flow field just before impact. Thus we are seeking to determine the motion in the regime where the fluid inertia is the dominant feature. In this context the moment of impact poses several difficulties. In the first instance the potential function becomes multivalued at the impact site. This discontinuity will be later identified with the circulation in the flow that persists in the toroidal geometry. Secondly, there is a jump in the magnitude of the normal derivative of the potential, $\partial\phi/\partial n$, across the impact site. From kinematical considerations, this discontinuity cannot persist after the impact. Thus we must give some consideration to the moment of impact.

First, though, we review the boundary integral method since it is this technique that will be modified to compute the motion of toroidal bubbles. We then give consideration to the impact of fluid surfaces in order that we may numerically undertake the transition to the toroidal geometry that occurs due to jet impact. After impact has occurred the flow domain is doubly connected and possesses a circulation. In order to implement the boundary integral method we introduce a cut in the flow domain so that we may consider it as simply connected. Across this cut the potential is discontinuous, the magnitude of the discontinuity equal to the circulation in the flow. We consider the motion of several toroidal bubbles and the computations suggest that, upon the

rebound of a toroidal bubble, the fluid flowing through the torus may thin sufficiently that the flow domain resumes singly connected topology. This is in accord with the experimental results of Vogel, Lauterborn & Timm (1989) which indicate that permanent vortex ring bubbles may be formed upon the second collapse of a transient cavity.

2. The boundary integral method

We suppose that a bubble undergoes some motion in a fluid and shall denote the domain occupied by the fluid as Ω, with $\partial\Omega$ signifying its boundary. The bubble surface, S, is a subset of $\partial\Omega$. We shall further denote by $\boldsymbol{n}$ the normal to $\partial\Omega$ and choose that it be directed exterior to Ω. We allow for the presence of a uniform gravitational field and choose a Cartesian set of axes, defined by the orthonormal basis $\boldsymbol{e}_x$, $\boldsymbol{e}_y$, $\boldsymbol{e}_z$, such that the gravitational acceleration is given by $\boldsymbol{g} = -g\boldsymbol{e}_z$. A schematic representation of this geometry is shown in figure 1.

We describe the fluid as inviscid and incompressible and the flow induced by the bubble's motion as irrotational. We introduce a velocity potential, ϕ, with ϕ satisfying Laplace's equation in Ω:

$$\nabla^2\phi = 0. \tag{2.1}$$

On $\partial\Omega$ appropriate boundary conditions are employed. There is no flow normal to a rigid boundary and the potential is assumed known at free surfaces. The Bernoulli equation is utilized to determine the evolution of free boundaries, that of significance in this study being the bubble surface. In our coordinate system the Bernoulli equation takes the form

$$\frac{\partial\phi}{\partial t} + \tfrac{1}{2}|\nabla\phi|^2 + p/\rho + g(z - z_0) = p_\infty/\rho. \tag{2.2}$$

In this expression t, ρ, p and p_∞ respectively denote the time, density, pressure and hydrostatic pressure at z_0. In this investigation surface tension is neglected.

We employ an elementary description of the bubble contents. We suppose that the bubble contents consist of the liquid vapour that exerts a constant partial pressure, p_c, throughout the lifetime of the bubble, and a non-condensible gas that we describe as ideal and undergoing adiabatic expansions. The partial pressure exerted by the non-condensible gas is thus given as a function of the volume, V, so that the pressure, p_b, inside the bubble is given by

$$p_b = p_c + p_0(V_0/V)^\gamma, \tag{2.3}$$

where the subscript 0 denotes initial quantities and γ is the ratio of specific heats. In this study we choose $\gamma = 1.4$. In the past, numerical investigations of transient cavity dynamics have neglected the presence of a non-condensible gas within the bubble, based upon the assumption that, particularly during the collapse of the bubble, the liquid vapour condenses sufficiently quickly that a constant pressure within the bubble is maintained. Much experimental evidence, however, indicates that the later stages of the bubble collapse proceed so quickly that this cannot occur. This is evidenced by the pronounced rebound of such bubbles, caused by the high pressure created as the vapour that does not condense is rapidly compressed in the very brief period about minimum volume (Vogel *et al.* 1989; Lauterborn 1982; Lauterborn & Bolle 1975; Benjamin & Ellis 1966). In the example of underwater explosion bubbles, the bubble contents are primarily composed of the non-condensible remnants of the detonation.

It is useful at this point to introduce a time and length scale, and a number of the physical parameters that characterize the motion. We choose the maximum bubble radius, R_m, as a lengthscale and $R_m(\rho/\Delta p)^{\frac{1}{2}}$ as a timescale. The potential scale is thus $R_m(\Delta p/\rho)^{\frac{1}{2}}$ and pressures are scaled with respect to $\Delta p = p_\infty - p_c$. Using this scaling the Bernoulli equation evaluated at the surface of the bubble becomes

$$\frac{\partial \phi}{\partial t} + \tfrac{1}{2}|\nabla\phi|^2 + \alpha(V_0/V)^\gamma + \delta^2(z - z_0) - 1 = 0, \tag{2.4}$$

where

$$\delta = (\rho g R_m/\Delta p)^{\frac{1}{2}} \tag{2.5}$$

is the buoyancy parameter, which provides a measure of the strength of the buoyancy force. In this paper we shall not consider cases where δ is non-zero, but retain the buoyancy term for completeness. Our principal concern is with motion in the neighbourhood of a plane rigid boundary. Supposing that the motion begins at some distance ξ_0 from the boundary, we define

$$\beta = \xi_0/R_m \tag{2.6}$$

as a geometry parameter, and this gives some measure of the influence of the flow induced by the presence of the boundary upon the bubble's motion (see Blake *et al.* 1986; Blake & Gibson 1987). Finally we note the parameter α defined as

$$\alpha = p_0/\Delta p. \tag{2.7}$$

We shall suppose that the bubble is initially spherical and of radius R_0. The motion of the bubble is driven from rest by the partial pressure exerted by the non-condensible gas and the parameter α provides some measure of the strength of this pressure. We choose our initial bubble radius, given the value of α, such that radial oscillations in an infinite fluid would give rise to a maximum radius of one (see Best & Kucera 1992).

Application of Green's theorem allows us to write the solution of Laplace's equation in the domain Ω as

$$c(\boldsymbol{p})\,\phi(\boldsymbol{p}) = \int_{\partial\Omega} \left(\frac{\partial \phi}{\partial n} G - \phi \frac{\partial G}{\partial n} \right) \mathrm{d}S, \tag{2.8}$$

with

$$c(\boldsymbol{p}) = \begin{cases} 2\pi, & \boldsymbol{p} \in \partial\Omega, \\ 4\pi, & \boldsymbol{p} \in \Omega \backslash \partial\Omega. \end{cases} \tag{2.9}$$

The surface $\partial\Omega$ is supposed to be everywhere smooth. The point $\boldsymbol{p}$ is somewhere in the flow domain and $\partial/\partial n \equiv \boldsymbol{n}\cdot\nabla$ is the normal derivative at the boundary. The Green's function is given by G and the notation $\Omega\backslash\partial\Omega$ denotes the complement of $\partial\Omega$ in Ω. We comment that if $\partial\Omega$ were not smooth (such as in cases where there are corners) then (2.8) remains valid, but the value of the function c at the points where the surface is not smooth would differ from 2π. It is a routine matter to determine the value of this function given the surface geometry. The reader may consult Seybert *et al.* (1985) for details.

In developing the boundary integral method for the solution of problems in bubble dynamics we note that the surface, $\partial\Omega$, that bounds the flow domain includes the bubble surface S. If we consider motion in an infinite fluid then $\partial\Omega$ is identically the surface of the bubble. In cases where the geometry of the flow domain is particularly simple we may circumvent the need to include boundaries, other than the bubble surface, in our description by appropriate choice of the Green's function. The geometry of particular relevance here is that of motion in the neighbourhood of a rigid

boundary. We may account for the presence of such a boundary by the addition of an image to the Green's function, in which case we need only take $\partial\Omega$ in (2.8) as the surface of the bubble. From a computational point of view this modification of the Green's function alleviates the necessity of having a description of the rigid boundary and evaluating integrals over this surface.

We suppose that at some time, t, the bubble geometry, S, and the potential on S are known. Equation (2.8) is then a Fredholm integral equation of the first kind for the normal fluid velocity, $\partial\phi/\partial n$, at the bubble surface. Solution for this quantity allows the fluid velocity at the bubble surface to be determined. Knowledge of this velocity allows the bubble surface at some short time, δt, later to be determined. The potential on the surface at $t+\delta t$ may similarly be determined and we may solve (2.8) for $\partial\phi/\partial n$ at $t+\delta t$. In this manner we iterate the solution for the flow field in time. In particular, if $\boldsymbol{X}$ denotes the position vector of some point on the bubble surface and $\boldsymbol{u}$ denotes the fluid velocity there, then solution of (2.8) allows determination of $\boldsymbol{u}$ and hence integration of the equation

$$\mathrm{d}\boldsymbol{X}/\mathrm{d}t = \boldsymbol{u}, \tag{2.10}$$

describing the motion of points on the bubble surface in the Lagrangian sense. The rate of change of the potential following some fluid element at the bubble surface is

$$\mathrm{d}\phi/\mathrm{d}t = \partial\phi/\partial t + |\nabla\phi|^2 = \tfrac{1}{2}|\nabla\phi|^2 - \alpha(V_0/V)^\gamma - \delta^2(z-z_0) + 1, \tag{2.11}$$

$\partial\phi/\partial t$ having been eliminated using (2.4). Since $|\nabla\phi|^2 (= |\boldsymbol{u}|^2)$ is known, (2.11) may be integrated simultaneously with (2.10), thus giving the potential on the bubble surface as a function of time.

The algorithm that is to be the basis for our study is that of Kucera (1993). To solve (2.8) Kucera (following Blake *et al.* 1986) employs a collocation method in an axisymmetric geometry. A set of $n+1$ nodes are chosen on the surface of the bubble, with the assumption of axisymmetric motion necessitating only the description of a curve in two dimensions. We denote the cylindrical coordinates of the ith node as (r_i, z_i) with $i \in \{0, 1, \ldots, n\}$. The surface of the bubble is then represented by a cubic spline, constrained to pass through the node points, with the spline parameter chosen as the arclength along the curve that is the bubble surface. Similarly, the potential over the surface S is represented using a cubic spline, parameterized with respect to the arclength. We represent $\partial\phi/\partial n$ on S linearly with respect to the arclength, its value at the nodes being the unknown quantities that we solve for. Collocation of (2.8) at the node points yields a linear system of equations for $\partial\phi/\partial n$ at the nodes, that is solved via the singular value decomposition. In collocating (2.8) at the nodes, the integration over the azimuthal angle is performed analytically, yielding expressions involving elliptic integrals of the first and second kind. The integration over the arclength is performed numerically using Gauss–Legendre quadrature formulae. When the integrand is singular, the logarithmic singularity is subtracted and an appropriate quadrature scheme is utilized to complete the integration. For details concerning these aspects the reader is referred to the work of Kucera (1993) and Taib (1985). We comment that, typically, Fredholm equations of the first kind lead to poorly conditioned systems of linear equations. In this case, however, the integrand exhibits a logarithmic singularity and this leads to a well-conditioned system. The method used here is advantageous in that the quantity of interest, $\partial\phi/\partial n$, is given directly. Other boundary integral formulations that lead to second-kind equations are possible and examples include those of Baker, Meiron & Orszag (1980, 1982, 1984) and Oguz & Prosperetti (1990).

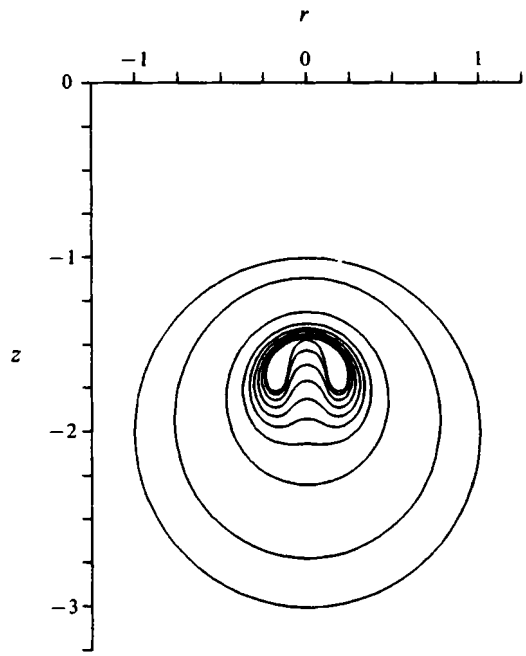

FIGURE 2. The collapse of a bubble characterized by $\beta = -2$, $\alpha = 100$ and $\delta = 0$. The times corresponding to successive profiles are: 1.1552 (outermost), 1.7789, 2.0357, 2.0835, 2.0992, 2.1096, 2.1184, 2.1263, 2.1332, 2.1382 (innermost).

Upon evaluating the fluid velocity at the node points, (2.10) and (2.11) are integrated in time using an Euler scheme with the time step chosen according to

$$\delta t = \frac{\Delta\phi}{\max_S(\frac{1}{2}|\nabla\phi|^2 + \alpha(V_0/V)^\gamma + \delta^2|z - z_0| + 1)}, \tag{2.12}$$

where $\Delta\phi$ is some constant. Application of this formula ensures that the change in potential at the nodes is bounded above by $\Delta\phi$ for each time step. In the computations presented here $\Delta\phi$ was chosen as 0.01. During the computation the mesh representing the bubble surface is redefined after every time step so that the nodes are evenly spaced with respect to the arclength. As the computation proceeds slight instabilities of a saw-tooth nature become evident in the bubble shape. To remove this instability the five-point smoothing formula first employed by Longuet-Higgins & Cokelet (1976) is applied every 5–20 iterations.

The performance of this algorithm applied to cavitation bubble motion has been investigated by Kucera (1993), and data relating to the performance are presented in that paper. Particular tests on the code include computation of the motion of a spherical cavity in an infinite fluid, and excellent agreement is found with the analytical solution of Rayleigh (1917). Furthermore, computations of jetting motion during collapse in the neighbourhood of a rigid boundary are in excellent agreement with the results of Blake *et al.* (1986).

We consider two example computations but note that a parametric study of the motion of bubbles whose contents are described by (2.3) has been recently undertaken by Best & Kucera (1992). The first is shown in figure 2 and is characterized by $\alpha = 100$, $\beta = -2$ and $\delta = 0$. The initial radius is 0.1651. Only the bubble shapes at successive times during the collapse phase are shown. During the growth phase the bubble

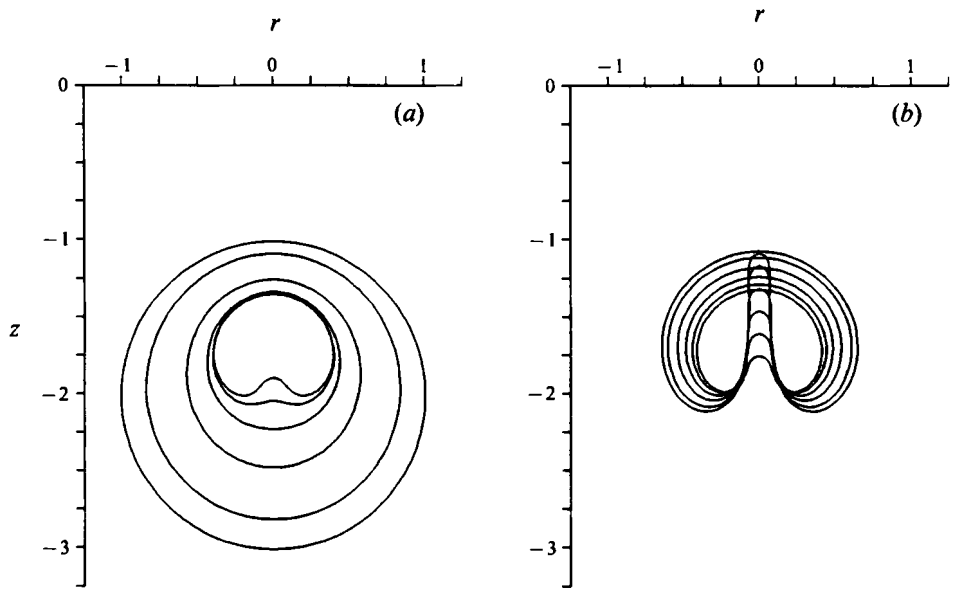

FIGURE 3. The collapse and rebound of a bubble characterized by $\beta = -2$, $\alpha = 10$ and $\delta = 0$. The times corresponding to successive profiles are: (*a*) Collapse phase: 1.2793 (outermost), 1.8604, 2.1936, 2.3146, 2.3644, 2.3945 (innermost). (*b*) Rebound phase: 2.4226 (innermost), 2.4535, 2.4895, 2.5327, 2.5860, 2.6225 (outermost).

qualitatively maintains a spherical shape to a good level of approximation. This characteristic depends, however, upon the proximity of the boundary. The bubble generally experiences some elongation along the axis of symmetry and experimental data on this aspect have been compiled by Vogel *et al.* (1989). Furthermore, the numerical study of Blake *et al.* (1986) showed that for motion in very close proximity to a rigid boundary, the bubble may deform significantly from spherical shape during the expansion phase. Upon collapse, the greater mobility of the fluid away from the boundary causes the surface of the bubble there to collapse faster than elsewhere, leading to the formation of a liquid jet that threads the bubble and ultimately impacts upon the far side of the bubble.

For this particular computation the number of elements, n, representing the bubble surface was equal to 32. In order to obtain some indication of the effect of smoothing the relative changes per smoothing operation in kinetic energy, ΔE, Kelvin impulse, ΔI, and bubble volume, ΔV, were evaluated. The mean absolute values of these changes are $\Delta E = 1.34 \times 10^{-4}$, $\Delta I = 1.85 \times 10^{-4}$ and $\Delta V = 1.48 \times 10^{-4}$. We note that all three quantities decreased due to smoothing, up until the time that the jet formed. Thereafter, the volume continued to decrease due to smoothing but the other quantities increased. These values indicate that, to a good degree of approximation, application of smoothing does not violate conservation of energy, momentum and mass, and further that smoothing does not alter the physics embodied in the mathematical model. The effect of mesh refinement may be illustrated by computing the quantities discussed above. For $n = 64$ the mean relative errors per smoothing operation are $\Delta E = 7.73 \times 10^{-6}$, $\Delta I = 1.10 \times 10^{-5}$ and $\Delta V = 9.05 \times 10^{-6}$. The computational effort for $n = 64$ is approximately four times that for the $n = 32$. For this reason, despite the order-of-magnitude smaller perturbations due to smoothing, the computations shown in this paper were carried out using $n = 32$.

Impact was considered to have occurred at the time step prior to that at which the

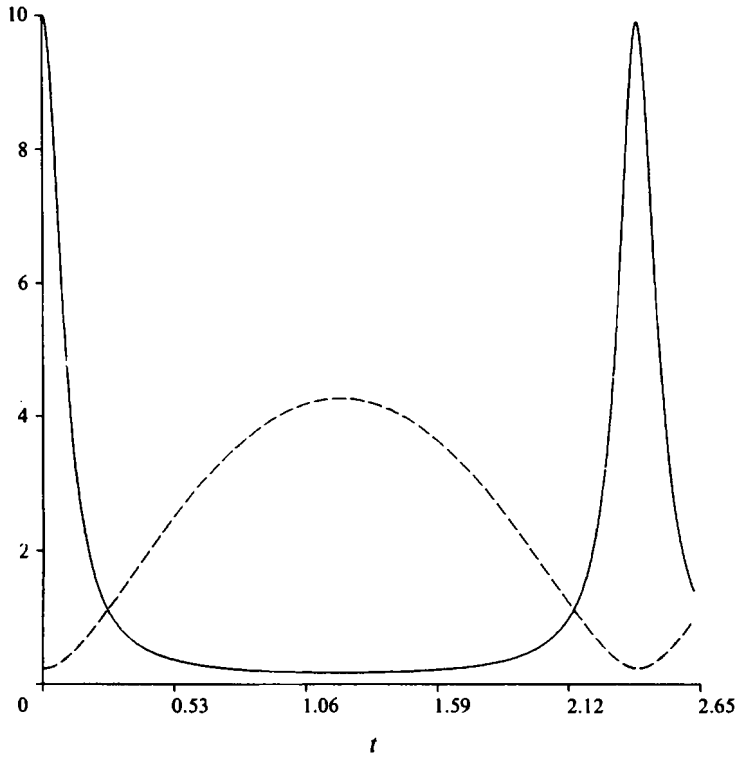

FIGURE 4. The pressure within the bubble (——) and the bubble volume (— —) as functions of time, for the motion depicted in figure 3.

distance between nodes 0 and n, denoted by Δs, becomes less than 1.0×10^{-2}. According to this criterion the time of impact here is 2.1382 with $\Delta s = 1.07 \times 10^{-2}$, and the smoothing was applied every 5 iterations. Approximately 1035 time iterations were required consuming about 60 minutes CPU time on a VAX 8700. As a further comment on algorithm performance, the time of impact for various smoothing intervals was computed. If we denote the smoothing interval by i_s then the time of impact for $n = 32$ is 2.1382 ($i_s = 5$), 2.1380 ($i_s = 10$) and 2.1379 ($i_s = 20$). For $n = 64$ the time of impact is 2.1379 ($i_s = 5$), 2.1378 ($i_s = 10$) and 2.1378 ($i_s = 20$). This variation is negligible compared to the lifetime of the bubble and is of the order of the error involved in setting a criterion that impact has occurred.

The second example is characterized by $\alpha = 10$, $\beta = -2$ and $\delta = 0$, and shown in figure 3. The initial radius is 0.3804. The pressure within the bubble and its volume are shown as functions of time in figure 4. In contrast to the previous case, the fluid velocities upon collapse are smaller and the high pressure generated by the decreasing bubble volume is sufficient to delay the full development of the jet until after the bubble has rebounded. In figure 3(*a*) we display the collapse phase of the motion and the elements of a jet directed towards the rigid boundary are evident at minimum volume. The rebound phase is shown in figure 3(*b*), and the momentum in the jet continues to drive the jet into the bubble as it re-expands, the decreasing bubble pressure assisting in this endeavour (figure 4). Again the computation is shown up until the time that the jet completely threads the bubble and impinges upon the far side.

In order to continue the computation beyond the time of impact a number of difficulties must be resolved. In the first instance the potential is discontinuous at the

impact site. Secondly, there is a jump in the magnitude of the normal fluid velocity across the impact site, but this discontinuity cannot persist after the impact. Thus we give some consideration to the moment of impact.

3. Evolution into a toroidal geometry

Consider the schematic representation of axisymmetric jet impact in figure 5. We suppose that the flow domain Ω collapses from a singly connected to a doubly connected topology via an impact over a surface T, with the remainder of the bubble surface denoted by S. We shall denote the upper part of this surface by T_+ and the lower part by T_-. In what follows, the subscript $\pm$ shall denote quantities evaluated on $T_\pm$. In particular, the unit normals to $T_\pm$, exterior to the flow domain, will be denoted by $\mathbf{n}_\pm$ and we note that these vectors are oppositely directed. We denote by superscripts i and f values immediately prior to, and immediately after the impact. If we let $\boldsymbol{t}$ be the position vector of an arbitrary point on $T(\equiv T_+ \cup T_-)$, then just prior to the impact ϕ and $\partial\phi/\partial n$ are, in general, discontinuous across T. We write

$$\phi_+^{\mathrm{i}}(\boldsymbol{t}) - \phi_-^{\mathrm{i}}(\boldsymbol{t}) = \Delta\phi(\boldsymbol{t}), \tag{3.1}$$

which is generally a non-zero function.

In considering the evolution into a toroidal geometry we must address the physical significance of these discontinuities and determine whether they can persist after impact. Let us first address the discontinuity in ϕ. As postulated by Benjamin & Ellis (1966) and others, the collapse of the flow domain into a doubly connected geometry will give rise to a flow with circulation. If the flow in the doubly connected domain possesses a circulation, Γ, we obtain its value by integrating the velocity around some closed curve that threads the torus;

$$\Gamma = \int_{\mathscr{C}} \boldsymbol{u}\cdot\mathrm{d}\boldsymbol{s} = \phi_1 - \phi_0, \tag{3.2}$$

where ϕ_1 and ϕ_0 are respectively the final and initial values of the potential on the curve $\mathscr{C}$, provided Laplace's equation is satisfied at all points on $\mathscr{C}$. Let us suppose, for convenience, that the initial point of $\mathscr{C}$ is somewhere on T and that the curve $\mathscr{C}$ proceeds from T_- to T_+. In order to perform this computation we require some information regarding the value of the potential on $T_\pm$ immediately after the impact has occurred.

The action of the impact is to deliver an impulse to the fluid. Since the fluid is incompressible the disturbances associated with this impulse are transmitted with infinite speed throughout the fluid and immediately establish the flow field in the toroidal geometry. Following the discussion in Batchelor (1967, pp. 471–474) we consider the momentum equation

$$\partial\boldsymbol{u}/\partial t + \boldsymbol{u}\cdot\nabla\boldsymbol{u} = -\nabla p/\rho - g\boldsymbol{e}_z. \tag{3.3}$$

During the short interval over which the impulse is delivered the fluid velocity may change in value discontinuously throughout the flow domain. However, during this change the values of the velocity and its spatial derivatives remain finite and are negligible compared to $\partial\boldsymbol{u}/\partial t$. Furthermore g is a constant, so that over the short interval during which the impulse is delivered we can write

$$\partial\boldsymbol{u}/\partial t = -\nabla p/\rho. \tag{3.4}$$

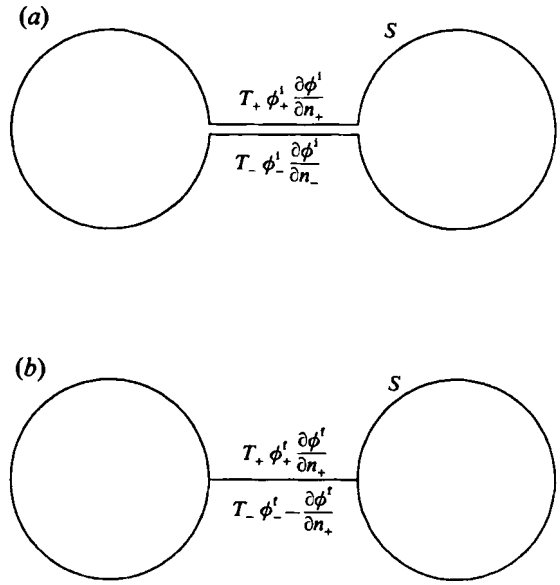

FIGURE 5. Schematic representation of the transition to the toroidal bubble geometry. The conditions at the surface T are shown (a) before impact and (b) after impact.

Integrating over the duration of the impulse we have

$$\boldsymbol{u}^f - \boldsymbol{u}^i = -\nabla \Pi/\rho, \tag{3.5}$$

where

$$\Pi = \int p \, dt \tag{3.6}$$

is the pressure impulse. This argument is valid when viscosity is included, but in our case where the fluid velocity is the gradient of a velocity potential we deduce from (3.5) that

$$\phi^f - \phi^i = -\Pi/\rho. \tag{3.7}$$

Applying (3.7) at T_+ and T_- we have

$$\left.\begin{aligned} \phi_+^f(t) - \phi_+^i(t) &= -\Pi_+/\rho, \\ \phi_-^f(t) - \phi_-^i(t) &= -\Pi_-/\rho. \end{aligned}\right\} \tag{3.8}$$

Since both surfaces experience a common pressure of the duration of the impact we have that $\Pi_+ = \Pi_-$, so

$$\Delta\phi^f(t) = \phi_+^f(t) - \phi_-^f(t) = \phi_+^i(t) - \phi_-^i(t) = \Delta\phi(t). \tag{3.9}$$

Hence we see that the value of Γ will, in general, depend upon the point on T that we choose to begin and end our curve, $\mathscr{C}$, of integration. If $\Delta\phi(t)$ is not uniform then the flow field that exists after the impact will be rotational. It is only in the case where $\Delta\phi$ is uniform that the flow field after impact is irrotational and possesses a circulation of $\Delta\phi$.

The consideration of the pressure impulse allows us to make further pertinent comments. On that part of the bubble surface denoted by S, the pressure for the duration of the impact is equal to p_b, the pressure inside the bubble that remains

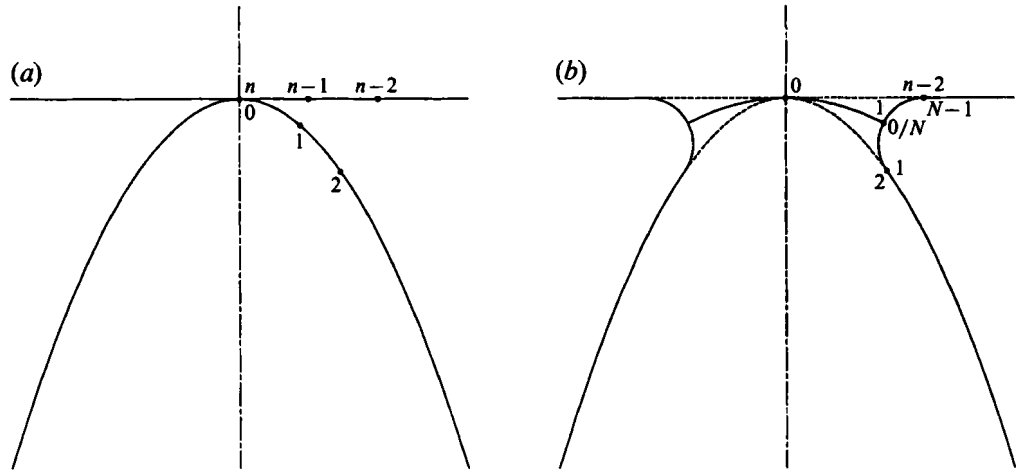

FIGURE 6. The numerical transition to the toroidal bubble geometry. The geometry is shown (*a*) immediately before and (*b*) immediately after impact.

constant for the duration of the impact. This is so because S is a free surface. Hence at some point on S the pressure impulse is

$$\Pi_S = \int p \, \mathrm{d}t = p_b \Delta t, \tag{3.10}$$

where Δt is the duration of the impact. In modelling the impact as an impulse we take the limit $\Delta t \to 0$ so that Π_S is equal to zero. Thus we deduce from (3.7) that for points on S the potential does not change due to the occurrence of the impact, a property that is exploited shortly.

The fluid velocity at T immediately after the impact is of interest noting that the absolute value of the normal velocities at T_+ and T_- must then be equal in magnitude. It is not possible to obtain a simple expression for this velocity, but we may derive an equation the solution of which allows the computation of this speed. We consider first the tangential component of the fluid velocity at T. Since the upper and lower surfaces of T experience a common pressure impulse at each point we have

$$\nabla \Pi_+(t) \cdot \tau(t) = \nabla \Pi_-(t) \cdot \tau(t), \tag{3.11}$$

where $\tau(t)$ is the tangent vector to T at t. Hence we have from (3.5) that

$$(u_+^t(t) - u_+^l(t)) \cdot \tau(t) = (u_-^t(t) - u_-^l(t)) \cdot \tau(t). \tag{3.12}$$

Thus at any point on T, the tangential components of the fluid velocity at T_+ and T_- change by the same amount due to the impact. If they are unequal before impact then this inequality will persist after impact and a vortex sheet will be created. This fact relates to the previous considerations regarding the line integral of the fluid velocity around some curve threading the torus. In the case where $\Delta\phi(t)$ is not uniform across T we deduced that the flow would be rotational. Such an example gives rise to a vortex sheet by the mechanism discussed above, this sheet being the source of the rotation in the flow field.

It is probable that the fluid velocity will exhibit singularities at the time of impact. The diagram of figure 5 does not illustrate fully what will probably be the circumstance in reality. At $S \cap T$, the bubble surface may not be smooth at impact, as is the case for the point impact that occurs when the jet penetrates the bubble, as shown in figure 6(*a*). This latter example is highly suggestive of singularities in the fluid velocity at points of

infinite surface curvature. The action of these is to smooth the surface and relieve the singularity. Expanding further on this point, suppose we consider a control volume about the impact surface in figure 5, that is collapsed down so that its upper and lower surfaces are respectively T_+ and T_-, and its sides are $S \cap T$. Just prior to impact, there is a finite rate of flow into the control volume through the surfaces T_+ and T_-, which must be matched by an outflow across the sides of the control volume ($S \cap T$). Since $S \cap T$ has zero area, the fluid velocity must be at least instantaneously singular to give the necessary finite rate of outflow from the control volume. This consideration indicates a possible fluid velocity singularity at $S \cap T$, even in the case where S is smooth where it meets T. In the example illustrated in figure 5, this singularity would cause a horizontally moving ring jet to arise from the contact surface.

In these circumstances, it is possible that the term $\boldsymbol{u}\cdot\nabla\boldsymbol{u}$ in (3.3) may not be negligible at points in $S \cap T$ for the duration of the impact. If we particularly address the case of ideal fluid flow, then integration of the Bernoulli equation over the duration of the impact yields

$$\phi^{\mathrm{f}}-\phi^{\mathrm{i}} = -\frac{\Pi}{\rho}-\frac{1}{2}\int |\nabla\phi|^2\,\mathrm{d}t, \tag{3.13}$$

if the last term is assumed only to be finite, in the limit of an impulsive impact. In the derivation of (3.9), it is assumed that the pressure is a single-valued function throughout the whole of the flow domain. The Bernoulli equation then suggests that each of the terms appearing in this equation are also single-valued functions throughout the flow domain, and particularly on T. Hence it is not unreasonable to assume that for those points in $S \cap T$, where the last term in (3.13) may possibly be non-zero, that $\int |\nabla\phi|_+^2\,\mathrm{d}t = \int |\nabla\phi|_-^2\,\mathrm{d}t$, and then (3.9) will follow for these points. The derivation of (3.12) follows also from this assumption, for those points in $S \cap T$. Since $\int |\nabla\phi|^2\,\mathrm{d}t$ is possibly only non-zero on $S \cap T$, then the change in the tangential component of the fluid velocity may be singular only at $S \cap T$, which is consistent with previous assertions. For the remainder of the analysis in this section to be applicable irrespective of any possible singularities in $\nabla\phi$, it is also necessary to assume that over a volume of measure zero, any singularity in $|\nabla\phi|^2$ integrates to zero. This property will then also be possessed by any component of $\nabla\phi$. This assumption is equivalent to stating that there cannot be non-zero kinetic energy bound in a volume of zero.

The preceding propositions must be confirmed by mathematical analysis, but at this stage the way to proceed in such an endeavour is unclear. In spite of this lack of knowledge of the detailed behaviour in the earliest times after jet impact, the considerations of this section may be used to guide the development of a numerical algorithm for the computation of toroidal bubble motion. Before proceeding with this, we require a boundary integral expression for the potential in the doubly connected flow geometry.

We have been able to show that the potential on S does not change as a result of the impact. We may exploit this knowledge to determine an equation which gives the normal derivative of the potential on S just after the impact. Making use of (2.8) we may write the potential at $\boldsymbol{p}\in S$ immediately prior to impact as

$$2\pi\phi^{\mathrm{i}}(\boldsymbol{p}) = \int_S\left(\frac{\partial\phi^{\mathrm{i}}}{\partial n}G-\phi^{\mathrm{i}}\frac{\partial G}{\partial n}\right)\mathrm{d}S+\int_T\left(\frac{\partial\phi^{\mathrm{i}}}{\partial n_+}G-\phi^{\mathrm{i}}_+\frac{\partial G}{\partial n_+}\right)\mathrm{d}S+\int_T\left(\frac{\partial\phi^{\mathrm{i}}}{\partial n_-}G-\phi^{\mathrm{i}}_-\frac{\partial G}{\partial n_-}\right)\mathrm{d}S. \tag{3.14}$$

Now $\partial G/\partial n_+ = -\partial G/\partial n_-$ so we have (see figure 5*a*)

$$2\pi\phi^{\mathrm{i}}(\boldsymbol{p}) = \int_S\left(\frac{\partial\phi^{\mathrm{i}}}{\partial n}G-\phi^{\mathrm{i}}\frac{\partial G}{\partial n}\right)\mathrm{d}S+\int_T\left(\frac{\partial\phi^{\mathrm{i}}}{\partial n_+}+\frac{\partial\phi^{\mathrm{i}}}{\partial n_-}\right)G\,\mathrm{d}S-\int_T\Delta\phi\frac{\partial G}{\partial n_+}\mathrm{d}S. \tag{3.15}$$

Immediately after the impact we may write the potential at $\boldsymbol{p}$ as

$$2\pi\phi^{\mathrm{f}}(\boldsymbol{p}) = \int_S \left(\frac{\partial\phi^{\mathrm{f}}}{\partial n}G - \phi^{\mathrm{f}}\frac{\partial G}{\partial n}\right)\mathrm{d}S - \int_T \Delta\phi^{\mathrm{f}}\frac{\partial G}{\partial n_+}\mathrm{d}S. \tag{3.16}$$

since $\partial\phi^{\mathrm{f}}/\partial n_+ = -\partial\phi^{\mathrm{f}}/\partial n_-$. We have shown that $\Delta\phi = \Delta\phi^{\mathrm{f}}$ and exploiting the fact that $\phi^{\mathrm{i}}(\boldsymbol{p}) = \phi^{\mathrm{f}}(\boldsymbol{p})$ for $\boldsymbol{p}\in S$ we obtain from (3.15) and (3.16) the relation

$$\int_S \frac{\partial\phi^{\mathrm{f}}}{\partial n}G\,\mathrm{d}S = \int_S \frac{\partial\phi^{\mathrm{i}}}{\partial n}G\,\mathrm{d}S + \int_T \left(\frac{\partial\phi^{\mathrm{i}}}{\partial n_+} + \frac{\partial\phi^{\mathrm{i}}}{\partial n_-}\right)G\,\mathrm{d}S, \tag{3.17}$$

which is satisfied at all points $\boldsymbol{p}\in S$. This is an integral equation from which $\partial\phi^{\mathrm{f}}/\partial n$ may be determined. In the toroidal geometry the expression for the potential is

$$c(\boldsymbol{p})\,\phi(\boldsymbol{p}) = \int_S \left(\frac{\partial\phi}{\partial n}G - \phi\frac{\partial G}{\partial n}\right)\mathrm{d}S - \int_T \Delta\phi\frac{\partial G}{\partial n_+}\mathrm{d}S, \tag{3.18}$$

with $c(\boldsymbol{p})$ given as in (2.9), provided $\boldsymbol{p}\notin T$. For $t\in T\ (\notin T\cap S)$ we have

$$4\pi\phi(t) = \int_S \left(\frac{\partial\phi}{\partial n}G - \phi\frac{\partial G}{\partial n}\right)\mathrm{d}S - \int_T \Delta\phi\frac{\partial G}{\partial n_+}\mathrm{d}S + 2\pi\Delta\phi(t). \tag{3.19}$$

Having obtained from (3.17) the value of $\partial\phi/\partial n$ on S after the impact, we may use (3.19) to evaluate the potential at points on T and (3.18) to evaluate the potential in the neighbourhood of T and hence determine the component of the fluid velocity normal to T.

We now turn our attention to the impact of the jet in the collapse of bubbles. In the idealized model impact occurs at one point in an axisymmetric geometry (figure 6*a*). Across this point the potential is discontinuous by an amount $\Delta\phi$, which corresponds to the circulation in the doubly connected flow topology. Since the surface over which the impact occurs is a point and $\Delta\phi$ is uniform over this surface there is no vortex sheet created by the impact. In order to describe such a flow using a boundary integral method we introduce a cut, T, in the domain Ω which allows us to once again consider it as singly connected. The initial cut consists of the point of impact, but as the flow develops, the geometry of the cut changes. At any point on the cut, however, the jump in potential across it is $\Delta\phi$ with the geometry as in figure 5(*b*) and the velocity potential is given by (3.18) and (3.19). In the limit of contact at a point the integral over T appearing in (3.17) vanishes so that over the surface S we have that $\partial\phi^{\mathrm{f}}/\partial n = \partial\phi^{\mathrm{i}}/\partial n$, except perhaps at points in $T\cap S$ where the normal is undefined. From our integral formulation the initial velocity of the impact point is indeterminate, as the surface T has been reduced to a set of measure zero. For the development of a numerical algorithm, however, this value is not necessary. Thus we have the theoretical base which will guide the numerical transition to a doubly connected flow geometry in the collapse of a bubble. We develop in the next section a boundary integral technique for the solution of (3.18) for $\partial\phi/\partial n$ at the bubble surface. The algorithm must be modified to include the term in this equation that involves integration over the cut T. This evaluation requires that the geometry of T is known. Thus we follow the cut as a material surface in the fluid. The details are discussed in the next section.

Before closing this discussion we make some remarks about the Kelvin impulse and kinetic energy of the fluid. The Kelvin impulse of the bubble is defined as

$$\boldsymbol{I} = \rho\oint_{S\cup T} \phi\boldsymbol{n}\,\mathrm{d}S. \tag{3.20}$$

We may write the impulse before impact as

$$\boldsymbol{I}^{\mathrm{i}} = \rho \int_S \phi^{\mathrm{i}} \boldsymbol{n}\, \mathrm{d}S + \rho \int_T \Delta\phi \boldsymbol{n}_+ \, \mathrm{d}S, \tag{3.21}$$

having exploited $\boldsymbol{n}_+ = -\boldsymbol{n}_-$ in evaluating the integral over T. The impulse immediately after impact is

$$\boldsymbol{I}^{\mathrm{f}} = \rho \int_S \phi^{\mathrm{f}} \boldsymbol{n}\, \mathrm{d}S + \rho \int_T \Delta\phi^{\mathrm{f}} \boldsymbol{n}_+ \, \mathrm{d}S. \tag{3.22}$$

Since $\phi^{\mathrm{i}} = \phi^{\mathrm{f}}$ on S and $\Delta\phi = \Delta\phi^{\mathrm{f}}$ on T, we see that

$$\boldsymbol{I}^{\mathrm{i}} = \boldsymbol{I}^{\mathrm{f}}, \tag{3.23}$$

and the impulse is conserved on impact. Note that this result is independent of whether the impact occurs at a point or over some surface, and is also independent of whether or not a vortex sheet is created by the impact. The kinetic energy of the flow is

$$E = \tfrac{1}{2}\rho \int_{\mathscr{V}} |\nabla\phi|^2 \, \mathrm{d}\mathscr{V}, \tag{3.24}$$

where $\mathscr{V}$ represents the volume of the flow domain. In general, since $\nabla\phi$ changes discontinuously throughout $\mathscr{V}$ due to the impact there is a discontinuous decrease in the kinetic energy of the fluid. In the case of point impact, though, $\nabla\phi$ is unchanged by the impact, except perhaps at the point of impact itself, which is a set of measure zero. In that case energy is conserved on impact. For impact over some surface the energy loss may manifest itself in the form of heat or acoustic energy.

4. The algorithm for computing the motion of a toroidal bubble

The motion of the bubble up until the time of impact may be computed using the boundary integral method described in §2. This computation yields the geometry of the bubble surface, the potential on it and the normal fluid velocity at this surface just prior to impact. The geometry just prior to impact is shown in figure 6(*a*). The number of nodes representing the bubble surface is $n+1$, with the initial node labelled as 0.

In order to numerically undertake the transition to a toroidal geometry we are guided by the considerations of the previous section. The impact occurs at the nodes 0 and n, so that the circulation in the flow that evolves is

$$\Delta\phi = \phi_n - \phi_0, \tag{4.1}$$

with the subscript denoting evaluation at the node. Over S the potential is unchanged by the impact and, owing to its occurrence at a point, the normal derivative of the potential is unchanged over S. Thus we may evaluate the fluid velocity at the node points $i = 1, 2, \ldots, n-1$ in the usual manner and determine their positions a short time, δt_i, later via the Euler time-stepping scheme. Similarly, the potential may be evaluated at these nodes at time $t + \delta t_i$ using the Euler scheme, where t here denotes the time of impact. The node 0 ($\equiv n$) is the initial cut, T, and the initial speed of this point is unknown. Regardless of what this initial speed is, it is finite, and in determining the position of this point at some later time by an Euler time-stepping scheme we can make its displacement arbitrarily small by letting our initial time step, δt_i, tend to zero. As $\delta t_i \to 0$ the displacement of the bubble surface and change in potential on it also tend to zero.

After this initial time step, however, we have no knowledge of where the cut, T,

meets the bubble surface. Although no analytic solution has been found for the early motion of the free surface about the impact point we might suppose that the very high surface curvature here gives rise to very high fluid velocities, the action of which is to immediately smooth the free surface. We perform this smoothing numerically by deleting the nodes $0, 1, n-1$ and n and fitting a smooth closed surface to the remaining nodes. Thus our bubble at time $t+\delta t_i$ is represented by $n-2$ nodes, including as a node the point where the cut meets the bubble. The point where the cut meets the bubble surface is taken to be halfway (with respect to arclength) between nodes 2 and $n-2$. This is the second node representing the cut, the first being the point at which impact occurs. The cut meets the bubble surface at right angles. This geometry is shown in figure 6(*b*).

We are now in a position to implement a boundary integral method to solve (3.18) for $\partial\phi/\partial n$ on S. The technique is unchanged from that discussed in §2 apart from the appearance of the term $\Delta\phi\int_T \partial G/\partial n_+ \,\mathrm{d}S$ in (3.18). The cut is represented by a cubic spline parameterized with respect to the arclength along the cut, and knowledge of its geometry in this form allows evaluation of this term. At this point we shall define $N = n-2$ and the number of nodes representing the bubble surface is then $N+1$, noting that, by this choice of N, nodes 0 and N are coincident. Similarly, the number of nodes representing the cut is N_c+1, with the node on the axis of symmetry taken as node 0. Since the potential is discontinuous at node $0/N$ we have that

$$\phi_N = \phi_0 + \Delta\phi \tag{4.2}$$

for the duration of the motion. In the boundary integral expression for the potential (equation (3.18)) the normal that appears is that to the surface $S \cup T$. Despite the existence of a normal to S at node $0/N$, the normal to $S \cup T$ is undefined there, and so then is $\partial\phi/\partial n$. Hence we choose to collocate at nodes $i = 1, 2, \ldots, N-1$. In order that the effective length of each element is the same, that joining nodes 0 and 1, and that joining nodes $N-1$ and N are half the length of all the others, reflecting the fact that we do not collocate at node $0/N$. The collocation method yields $\partial\phi/\partial n$ at the surface of the bubble and upon evaluation of the fluid velocity there we may determine the positions of, and potential at each node at some small time interval later using the Euler integration scheme.

Despite choosing not to collocate at node $0/N$, knowledge of the whereabouts of this node is essential to the computation as it defines that point on the bubble surface at which ϕ is discontinuous. Although $\partial\phi/\partial n$ is undefined at node $0/N$ we may assign it a value here, and the appropriate value is the limit of $\partial\phi/\partial n$ as we approach the node along S. This value is then the component of the fluid velocity normal to S, noting that despite the discontinuity in ϕ here, the fluid velocity is everywhere continuous, so that the limit we choose is independent of the direction of approach along S. We evaluate the appropriate limiting value by linear interpolation since we have chosen a linear representation for $\partial\phi/\partial n$ as discussed in §2.

In order to evaluate $\Delta\phi\int_T \partial G/\partial n_+ \,\mathrm{d}S$ we must know the whereabouts of the cut, T, so we follow its motion throughout the computation and this necessitates a knowledge of the fluid velocity normal to this surface. We obtain this velocity as follows. Let $\boldsymbol{n}$ denote the normal to T at some point t, with $\boldsymbol{n}$ directed interior to the fluid on T_+. If we further let $\delta\tau$ be some small distance then we can obtain a second-order finite difference approximation to the normal fluid velocity at T via

$$\nabla\phi\cdot\boldsymbol{n} \approx \frac{1}{2}\left[\frac{\phi(t+n\delta\tau)-\phi_+(t)}{\delta\tau}+\frac{\phi_-(t)-\phi(t-n\delta\tau)}{\delta\tau}\right], \tag{4.3}$$

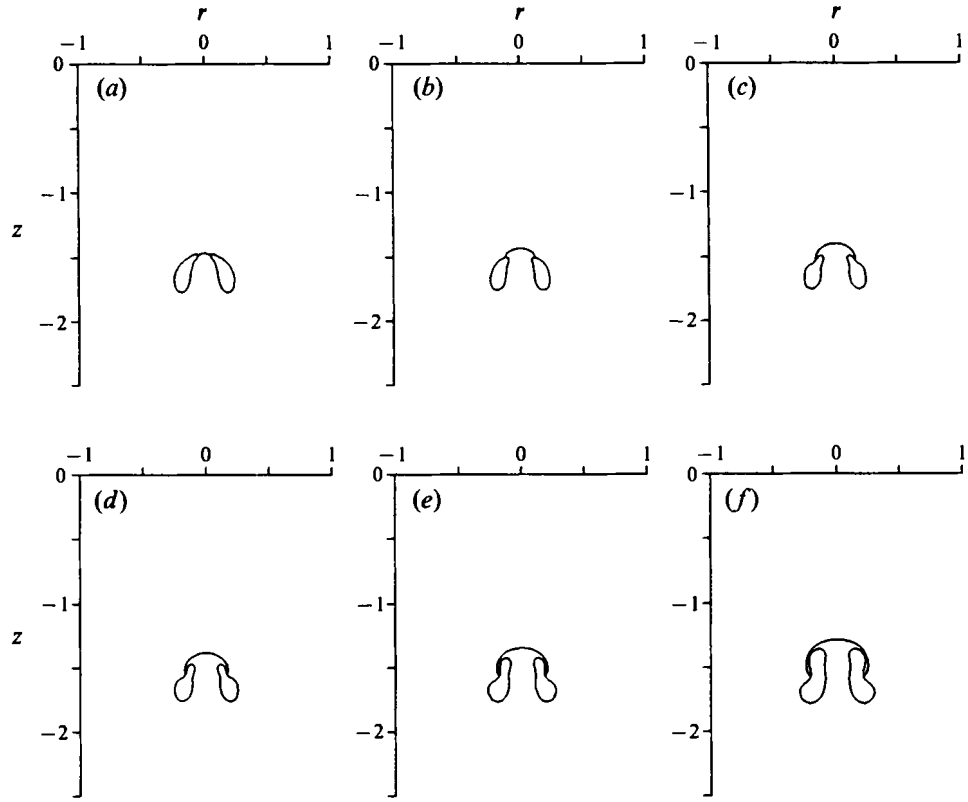

FIGURE 7(*a–f*). For caption see facing page.

but noting that

$$\phi_+(t) = \phi_-(t) + \Delta\phi, \tag{4.4}$$

this becomes

$$\nabla\phi \cdot \boldsymbol{n} \approx \frac{\phi(t+n\delta\tau) - \phi(t-n\delta\tau) - \Delta\phi}{2\delta\tau}. \tag{4.5}$$

In the computations presented here $\delta\tau$ was chosen to be 0.005. Note that we have avoided the need to calculate the potential on the surface T itself. With this expression for the normal velocity we may propagate nodes on T along their normals, using the Euler scheme, to determine the position of this surface a small interval of time, δt, later. Note that we are not following the motion of fluid particles at T. To do so would require knowledge of the tangential component of the fluid velocity, which could be obtained, but at the expense of significant computation. Since only the geometry of this surface is required the extra computational effort needed to follow points on T in a Lagrangian fashion is seen to be superfluous. In any case, we are following the motion of T as a material surface in the fluid and, as we shall see shortly, this provides considerable assistance in visualization of the flow. As the computation proceeds in time the length of the cut increases. Thus nodes are added in order that this surface remains adequately resolved. An appropriate strategy is to insert an extra node when the mean spacing between nodes becomes greater than some maximum distance $\Delta\xi_c$. In the computations presented here $\Delta\xi_c = 0.05$.

Every 5–15 iterations it is necessary to smooth the bubble surface, the cut surface and the potential on S as discussed in §2. In order to apply the smoothing formula to

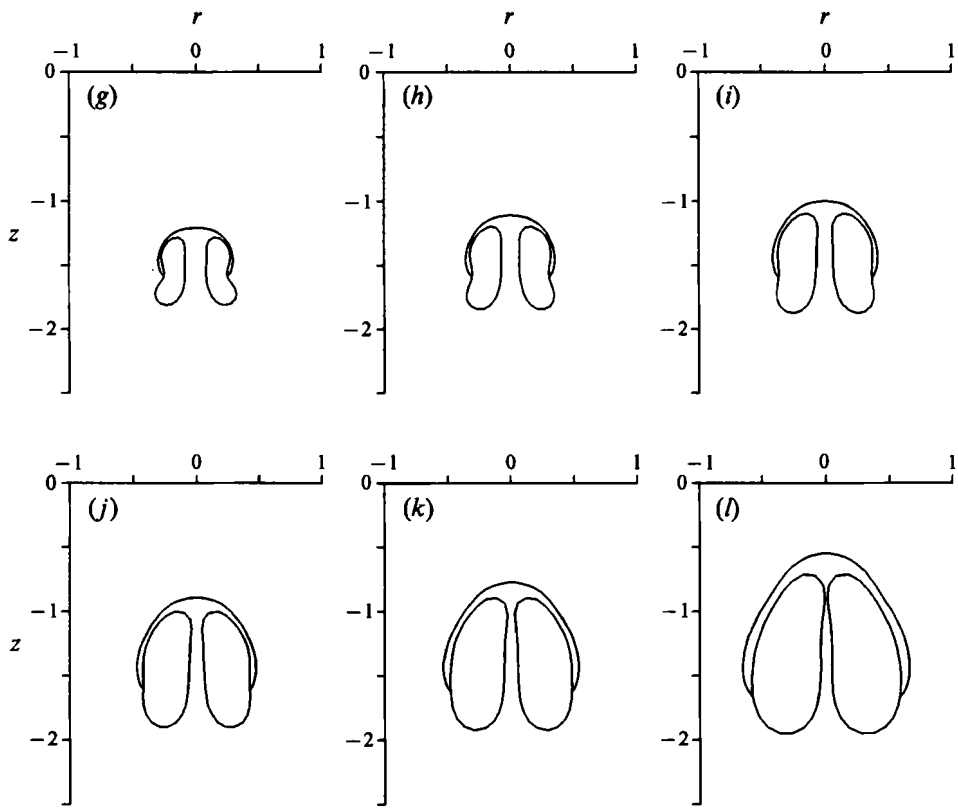

FIGURE 7. The motion of the toroidal bubble that evolves from the collapse of a bubble characterized by $\beta = -2.0$, $\delta = 0$, $\alpha = 100$. The circulation is $\Delta\phi = -4.185$. (*a*) $t = 2.1382$, (*b*) 2.1425, (*c*) 2.1478, (*d*) 2.1511, (*e*) 2.1565, (*f*) 2.1655, (*g*) 2.1784, (*h*) 2.1950, (*i*) 2.2162, (*j*) 2.2398, (*k*) 2.2688, (*l*) 2.3336.

the potential at nodes $N-1$ and 1, where application of the five-point formula includes points on the other side of the discontinuity in ϕ, those points on the other side are artificially redefined by the addition (or subtraction) of $\Delta\phi$ for use in the formula. After applying the smoothing formula to nodes $1 \ldots N-1$, node $0/N$ is taken to be halfway, with respect to arclength, between nodes 1 and $N-1$. When smoothing the cut, node N_c is considered as fixed, having already experienced smoothing as part of S. In order to apply the formula at node N_c-1 an artificial node N_c+1 is defined as the reflection of node N_c-1 about the plane tangent to the bubble surface at node N_c. This choice is made to preserve the orthogonality of the cut and bubble surface at this point. This imposition of orthogonality is artificial as these two material surfaces will not remain orthogonal as the motion proceeds. However, imposing orthogonality both via clamping the cut spline and application of the smoothing formula assists in making the code more robust. A series of test computations were carried out using the free end, or not-a-knot end condition where the cut spline meets the bubble surface (see DeBoor 1978). These led to computed bubble and cut geometries almost indistinguishable from those presented here. However, great care had to be taken in setting the frequency with which new nodes were inserted into the cut to ensure that the cut did not cross the bubble surface near to the point where the cut meets the bubble. The imposition of orthogonality of the cut and bubble surface alleviated this to a certain extent, and the error in the computed cut shape was negligible. Since the cut may be deformed arbitrarily throughout the flow domain the imposition of orthogonality of cut and

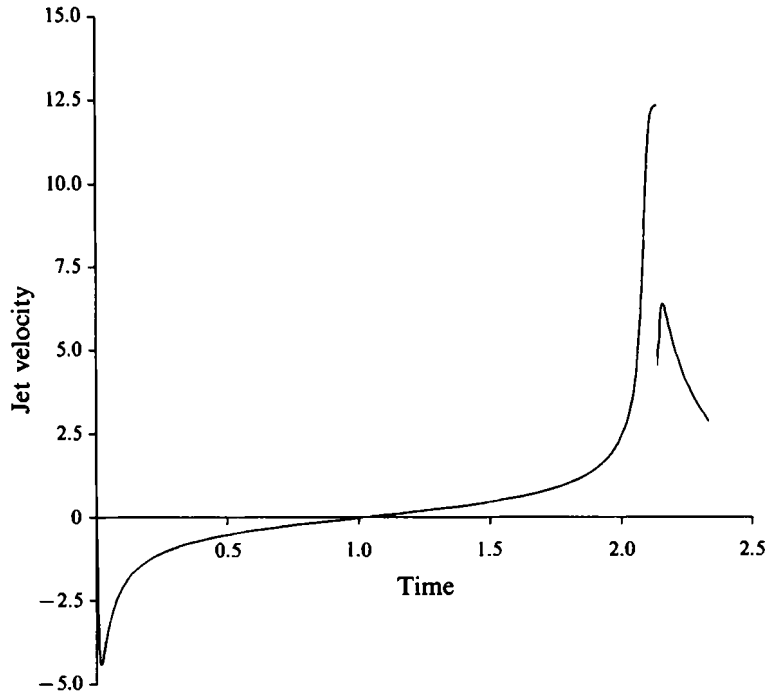

FIGURE 8. The jet tip velocity as a function of time for bubble motion characterized by $\beta = -2.0$, $\delta = 0$, $\alpha = 100$. The curve is discontinuous at the time that the transition to the toroidal geometry occurs. After this time the velocity plotted is that of the point on the cut, on the axis of symmetry.

bubble surface causes no error in the computed bubble shape. When smoothing points near the axis, artificial cut nodes -2 and -1, consisting of cut nodes 2 and 1 respectively reflected about the axis of symmetry, are used to facilitate smoothing of cut nodes 0 and 1. In the case where less than three nodes represent the cut no smoothing is performed. The mesh is redefined after every time step so that the nodes representing the bubble surface and those representing the cut are evenly spaced, noting that the spacing on the cut is not necessarily the same as the spacing on the bubble.

We conclude this section by making a comment of a mathematical nature. The cut, T, may be deformed throughout the flow field into any geometry that we choose. In order to interpret our results in view of recent experimental results we have followed T as a material surface. Equivalently we could proceed by redefining the potential throughout the fluid in order that the geometry of T is particularly simple.

5. Example computations of the motion of toroidal bubbles

The first example of toroidal bubble motion that we shall consider is for a bubble characterized by $\beta = -2.0$, $\delta = 0$, $\alpha = 100$. This example was considered in §2 and the motion up until the time of impact is shown in figure 2. The time of impact is taken as 2.1382 and the circulation is $\Delta\phi = -4.185$. The computed motion is shown in figure 7. The jet tip velocity is shown in figure 8, with the velocity of the uppermost point of the cut shown as this velocity for times after the impact. The centroid position as a function of time is illustrated in figure 9, the small discontinuity in this curve at the time of impact being purely a feature of the numerical transition to a toroidal geometry.

After the impact has occurred the fluid flows through the torus at a reduced speed.

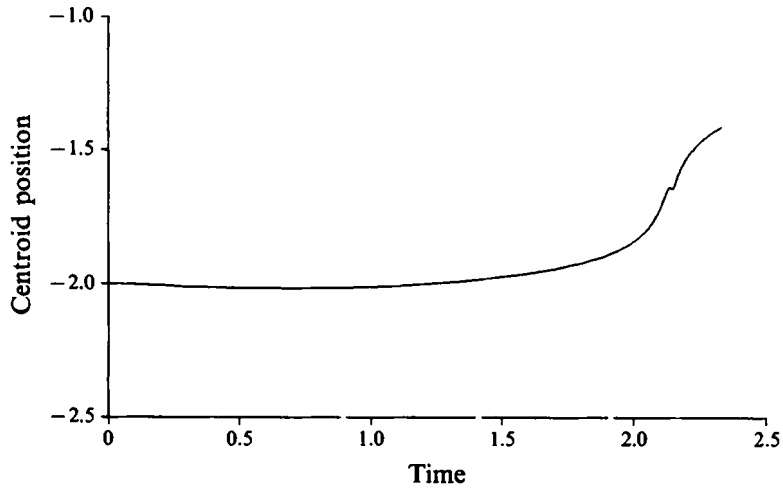

FIGURE 9. The centroid position as a function of time for bubble motion characterized by $\beta = -2.0$, $\delta = 0$, $\alpha = 100$. The curve is discontinuous at the time that the transition to the toroidal geometry occurs.

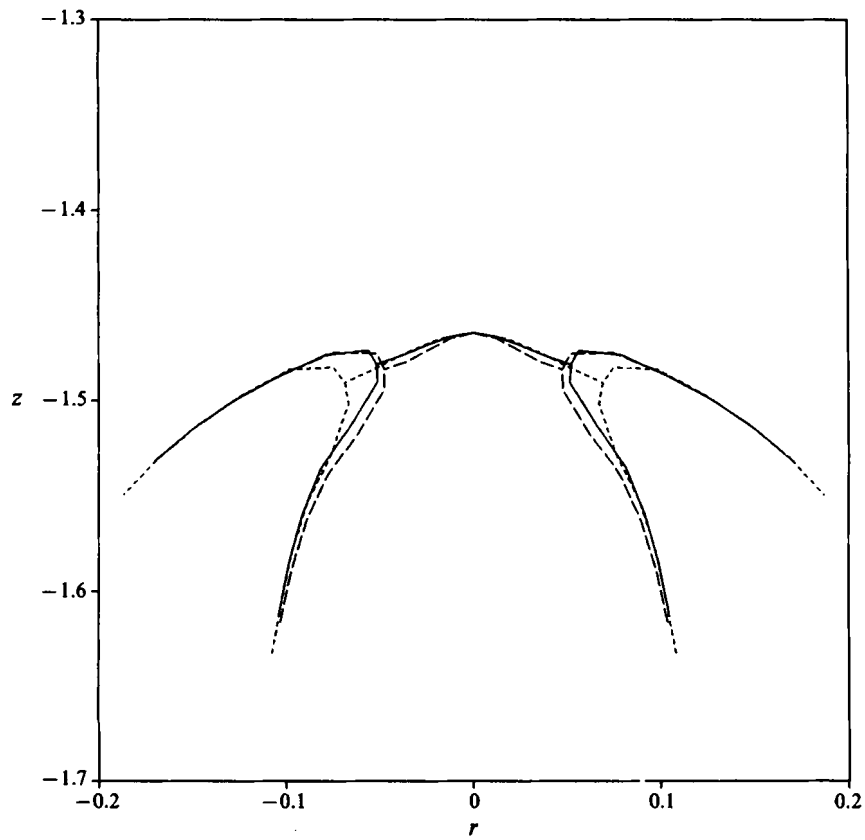

FIGURE 10. Three different initial toroidal bubble geometries: ——, $\Delta s = 1.07 \times 10^{-2}$, $\Delta\phi = -4.185$, nodes $n, n-1, 1, 0$ deleted; ——, $\Delta s = 2.08 \times 10^{-2}$, $\Delta\phi = -4.119$, nodes $n, n-1, 1, 0$ deleted; – – –, $\Delta s = 1.07 \times 10^{-2}$, $\Delta\phi = -4.185$, nodes $n, n-1, n-2, 2, 1, 0$ deleted.

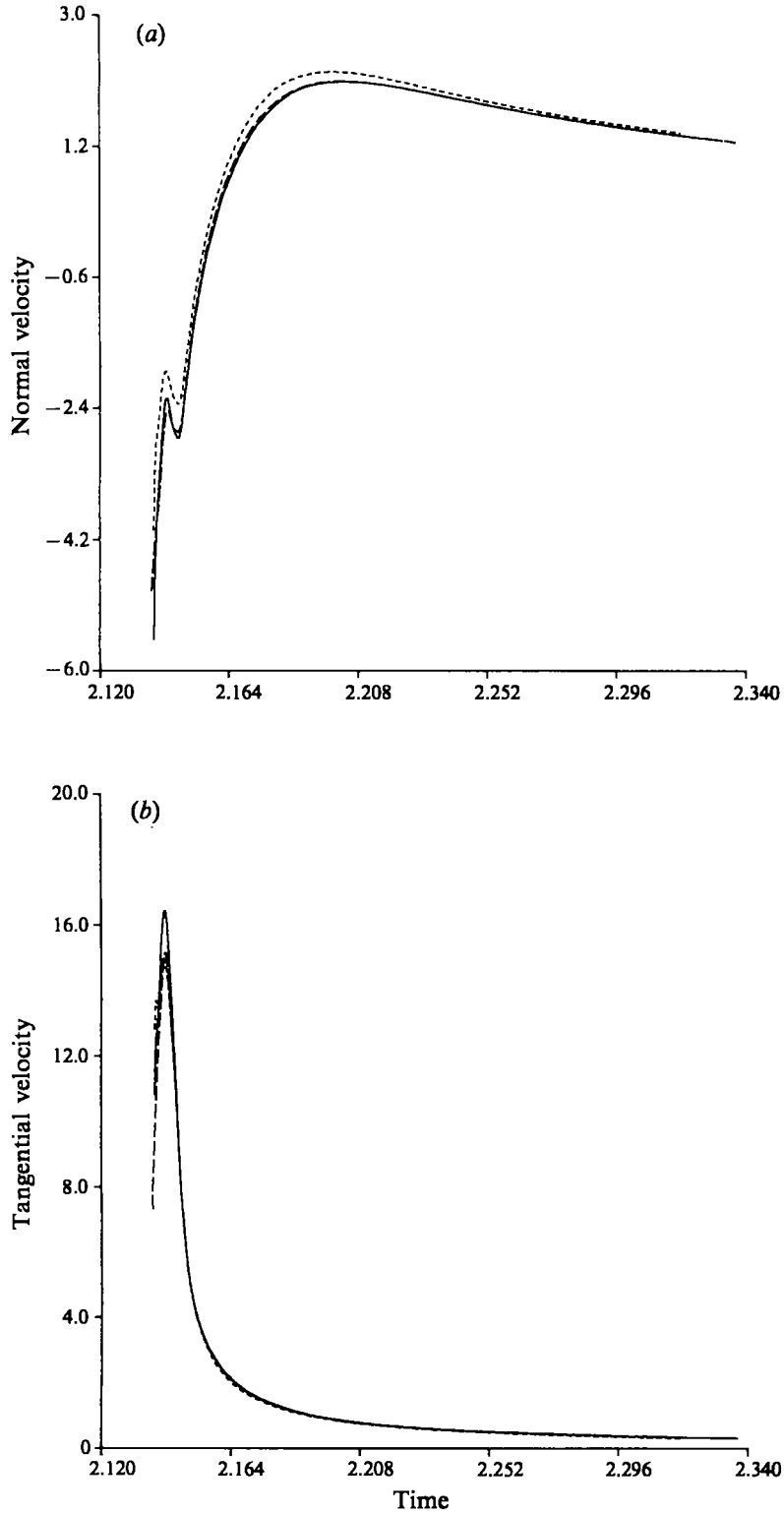

FIGURE 11. (*a*) The normal and (*b*) the tangential fluid velocity at the point where the cut meets the bubble surface, for each of the three initial geometries depicted in figure 10.

In this case the initial speed of the cut is approximately equal to the average of the fluid velocities at the upper and lower impact surfaces just prior to impact. This observation is in accord with the fact that the jet impact is a momentum-conserving interaction. Over the impacting surfaces an equal and opposite impulse is delivered. The effect upon the jet is to discontinuously decrease its velocity. Similarly, the effect upon the nearly stationary side of the bubble into which the jet impacts is to increase its speed, so that the two contacting surfaces then move with a common velocity. The bubble continues to collapse after impact and the speed of the tip of the cut increases as fluid is drawn in by this collapse. The rebound of the bubble then slows this motion. The very rapid change in the fluid acceleration here is characteristic of the rebound of bubbles whose contents are described using the pressure law of (2.3). This behaviour is particularly evident in the case of large-amplitude oscillations of spherical bubbles described by the Rayleigh–Plesset equation, and is caused by the rapid rise in the bubble pressure upon collapse changing the direction of the bubble surface motion over a very short interval of time. We further note that the collapse is characterized by the fast migration of the bubble centroid towards the rigid boundary. After impact migration continues towards the boundary but slows as the bubble re-expands. The circulation in the velocity field manifests itself in a flow of fluid around the torus that is the bubble. This initial flow around impinges upon the bubble surface forming a depression that travels around the side of the bubble. As the bubble re-expands, however, this depression vanishes.

It is recognized that the numerical transition to a toroidal geometry is somewhat *ad hoc*. In order, then, to gain some confidence that the computations presented here represent a plausible prediction of the real behaviour a number of convergence studies were carried out with respect to the parameters characterizing the initial insertion of a cut. The results for three different initial conditions are shown. For the results presented thus far, the distance between the upper and lower node at impact was $\Delta s = 1.07 \times 10^{-2}$, and the nodes $n, n-1, 1, 0$ were removed and the cut then inserted as described previously. We also show here the results for this value of Δs, but with nodes $n, n-1, n-2, 2, 1, 0$ removed. A further variation is the example where $\Delta s = 2.08 \times 10^{-2}$ with nodes $n, n-1, 1, 0$ removed. In this latter case the circulation is $\Delta\phi = -4.119$, the time of impact is 2.1374 and the point on the cut on the axis of symmetry is taken to be the node on the upper surface. These three different initial geometries are shown in figure 10.

The quantities evaluated to indicate the invariance of the subsequent behaviour to these variations consist of the normal and tangential components of the fluid velocity, at the point where the cut meets the bubble surface. These velocities are shown in figures 11(*a*) and 11(*b*) respectively, and were chosen because the point where T and S meet is the only one on the bubble surface that is followed with the fluid. The significant variation is for the example where nodes $n, n-1, n-2, 2, 1, 0$ were removed. The lifetime was reduced in this case, but we can explain this occurrence by noting that the removal of the extra nodes has the effect of advancing the bubble shape discontinuously in time. These results indicate that the computed motion of the toroidal bubble is essentially independent of the parameters used to define the initial toroidal bubble, as long as they are varied reasonably.

To consider the effect of smoothing and mesh refinement upon the computation of toroidal bubble motion ΔI and ΔV were computed, as in §2. The kinetic energy was not computed as the value depends upon the cut utilized. (See Batchelor 1967, pp. 112–114, for a discussion of this. The potential may be decomposed into the sum of a single-valued and cyclic potential in order to define the kinetic energy uniquely in terms of surface integrals. Investigations to date indicate that performing this decomposition on

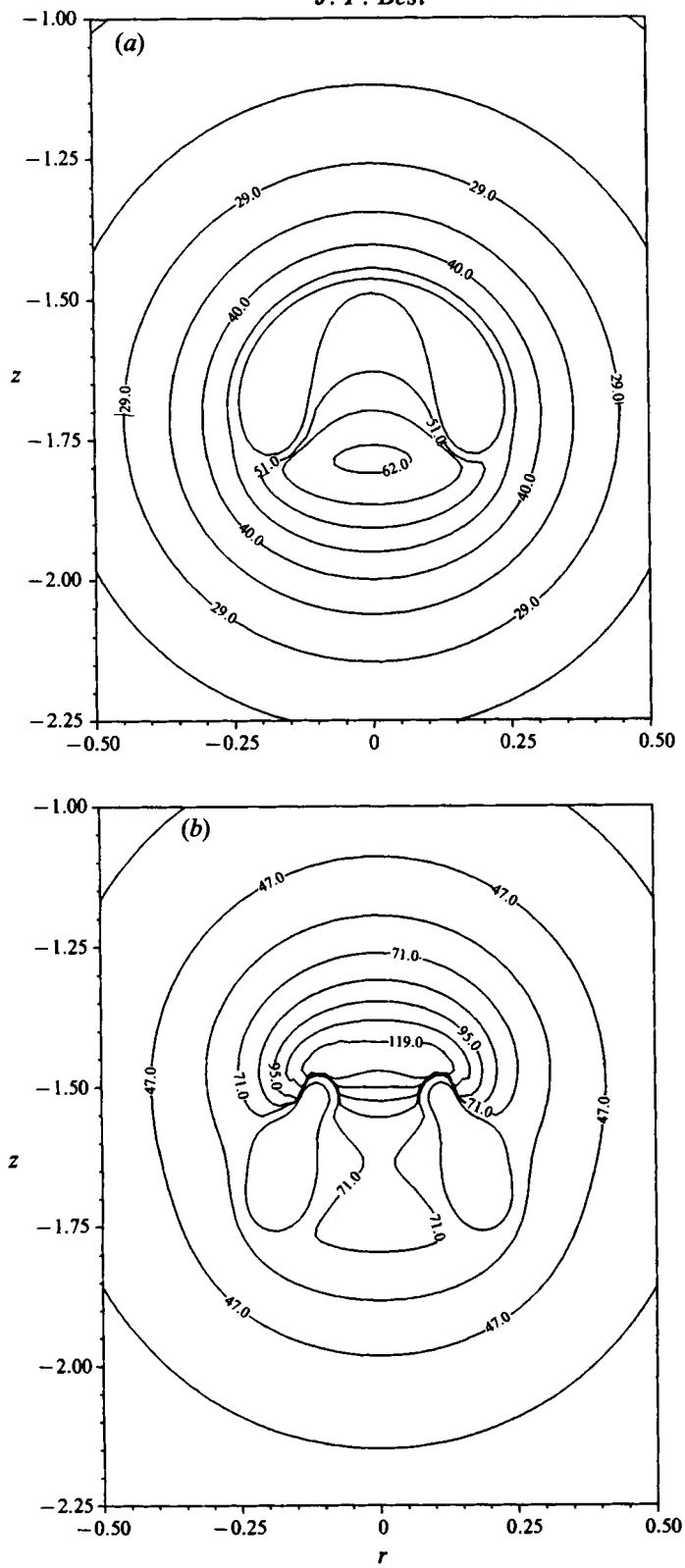

FIGURE 12. For caption see facing page.

a numerically computed potential function introduces large errors.) For the toroidal bubble that evolves from a singly connected bubble with $n = 32$ we have $\Delta I = 8.70 \times 10^{-4}$ and $\Delta V = 1.60 \times 10^{-3}$ with ΔI generally positive and ΔV generally negative. For $n = 64$, $\Delta I = 4.09 \times 10^{-4}$ and $\Delta V = 1.68 \times 10^{-4}$. These values indicate that momentum and mass are essentially conserved by the smoothing operation, although for long run times the accumulation of error may become significant. We further notice that the degree of improvement attainable by doubling n is not as good as in the case of the singly connected bubble. All subsequent computations of toroidal bubbles utilized $n = 32$ and this example required approximately 1240 iterations and 137 minutes CPU time on a VAX 8700. At the end of this particular computation 30 nodes represented the cut.

It is most relevant to consider the contrasting character of the pressure field in the fluid before and after the transition to the toroidal geometry, and this is computed using the Bernoulli equation. The pressure field just prior to impact ($t = 2.1370$) is shown in figure 12(*a*), and just after impact ($t = 2.1470$) in figure 12(*b*). Defining forwards as the direction of travel of the jet, this figure reveals a transition in the point of peak pressure from behind the bubble to ahead. Before the impact, the peak of pressure behind the bubble is the agent that drives the jet, but after impact this peak becomes located ahead of the bubble, its action being to decelerate the rush of the fluid through the torus towards the wall, and drive the motion of the fluid around the bubble. This finding is significant in assessing possible mechanisms for damage to boundaries due to cavitation or underwater explosion bubble collapse. It is apparent that even if the collapse is not so close to the boundary that we have water hammer impact pressures, the transition to the toroidal geometry creates a region of very high pressure in the fluid between the bubble and the boundary, leading to a loading of the boundary. For this example we have further computed the pressure at the rigid boundary just prior to, and just after impact, and this is shown in figure 13. Even though the bubble collapse is somewhat remote from the rigid boundary, the pressure experienced at the boundary is increased by over 50% due to the impact and the pressure distribution shows larger radial gradients.

We compare this result with the motion of a toroidal bubble characterized by $\beta = -1.5$, $\delta = 0$, $\alpha = 100$, as shown in figure 14. The motion prior to complete penetration by the jet is very similar in character to that illustrated in figure 2; however, owing to the closer proximity of the boundary in this case, the jet formed is broader but moving with lower speed at impact. The circulation in this example is $\Delta\phi = -4.629$. The motion after impact shares many features with the previous example and we are able to here follow the motion up until the time that the fluid initially in the jet has flowed completely around the bubble. A difference of some significance is that in the first example the central region through the torus thins and we propose that the fluid here disconnects and the flow domain resumes a simply connected topology, whereas in this case the initial breadth of the jet creates a broader central region through the torus and no mechanism for disconnection in this case is apparent. In the first example, neglected physical effects such as surface tension and pressure fluctuations within the bubble will accelerate the disconnection of fluid flowing through the torus.

FIGURE 12. The pressure field in the fluid computed (*a*) just before and (*b*) just after the transition to a toroidal geometry. The motion is characterized by $\beta = -2$, $\alpha = 100$, and $\delta = 0$. The times are (*a*) $t = 2.1370$ and (*b*) $t = 2.1470$. The isobars are at equally spaced pressure intervals. In (*a*), the pressure at the innermost contour is 62.0 and at the outermost contour is 18.0. In (*b*), the pressure at the innermost contour is 119.0 and at the outermost contour is 35.0.

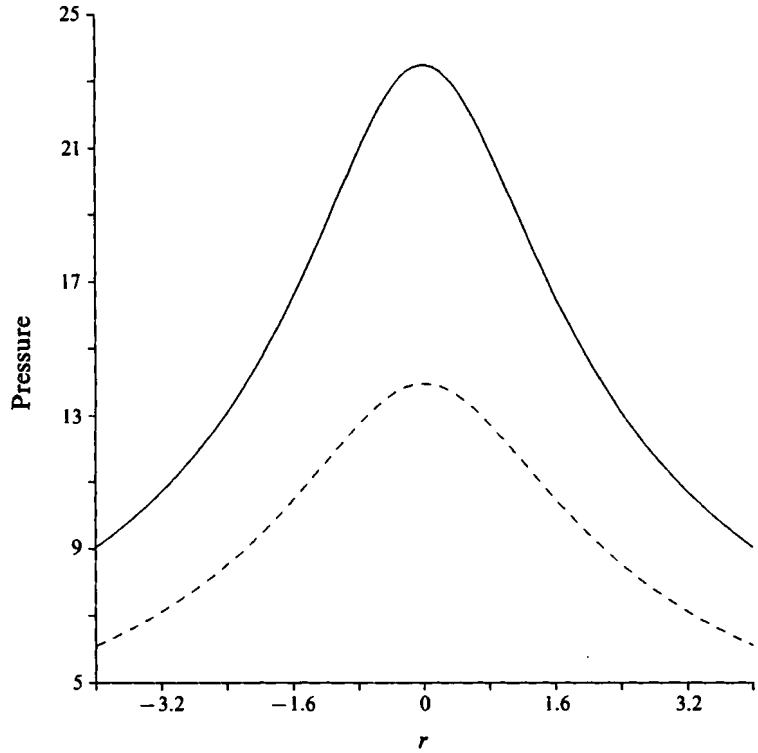

FIGURE 13. The pressure at the rigid boundary just prior to (dashed curve, $t = 2.1370$) and just after (solid curve, $t = 2.1470$) the transition to the toroidal geometry that occurs during motion characterized by $\beta = -2$, $\alpha = 100$ and $\delta = 0$.

In both of these examples the bubble continues to collapse after jet penetration, until the pressure inside is sufficiently high that further collapse is arrested and rebound occurs. In view of this it is interesting to consider an example in which jet impact occurs after rebound. The example we consider is characterized by $\beta = -2.0$, $\delta = 0$, $\alpha = 10$, the collapse and rebound of the connected bubble discussed in §2. The jet at impact is slowing and the circulation in this case is given by $\Delta\phi = -2.304$. The motion of the toroidal bubble is shown in figure 15 and since the circulation is low in this case the fluid flowing through the torus tends to continue flowing forward in preference to flowing around the bubble. It again appears that the fluid flowing through the bubble will disconnect.

We consider this example in the context of the recent experimental results of Vogel *et al.* (1989). In that work bubbles were generated by a laser in a fluid possessing a temperature gradient, so that the fluid in the jet is at a different temperature to the fluid into which the jet impacts. The fluid at different temperature has a different refractive index and is thus visible by a schlieren technique. Some of these results indicate profiles similar to those computed here (figure 24*a* from that paper), noting that such a visualization technique would give rise to an image of a bubble, with a cap corresponding to the cut computed here. Other results show what appear to be very sharp jets penetrating a large distance beyond the bubble (figure 7*a* from that paper). In such examples this structure does not usually become evident until after the bubble has rebounded. The computational results just presented indicate a cut geometry protruding above the bubble in such cases, but this geometry lacks the sharpness evident in the experimental results.

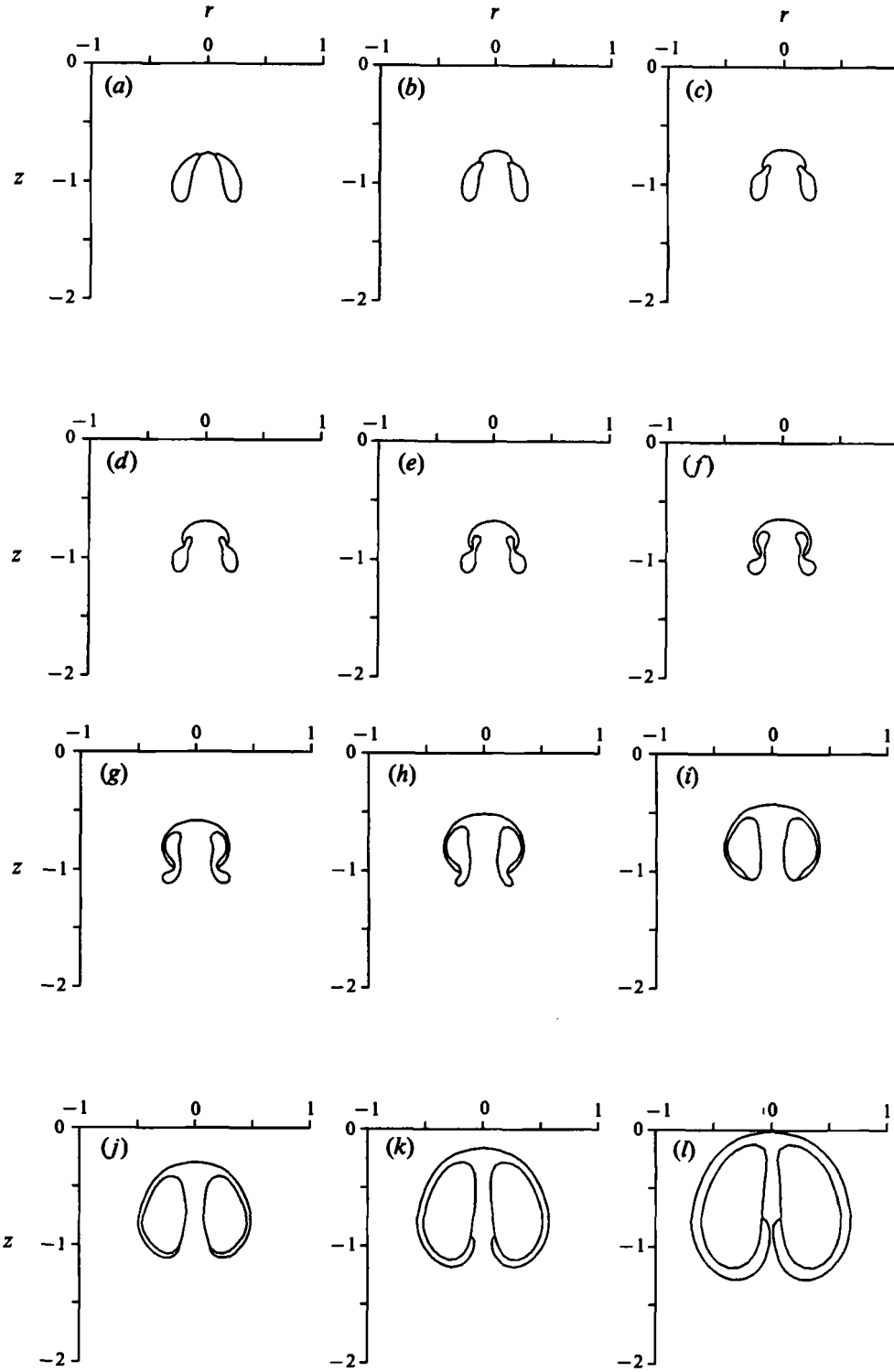

FIGURE 14. The motion of the toroidal bubble that evolves from the collapse of a bubble characterized by $\beta = -1.5$, $\alpha = 100$ and $\delta = 0$. The circulation is $\Delta\phi = -4.629$. (*a*) $t = 2.1894$, (*b*) 2.1958, (*c*) 2.2020, (*d*) 2.2047, (*e*) 2.2084, (*f*) 2.2151, (*g*) 2.2256, (*h*) 2.2394, (*i*) 2.2581, (*j*) 2.2862, (*k*) 2.3235, (*l*) 2.3857.

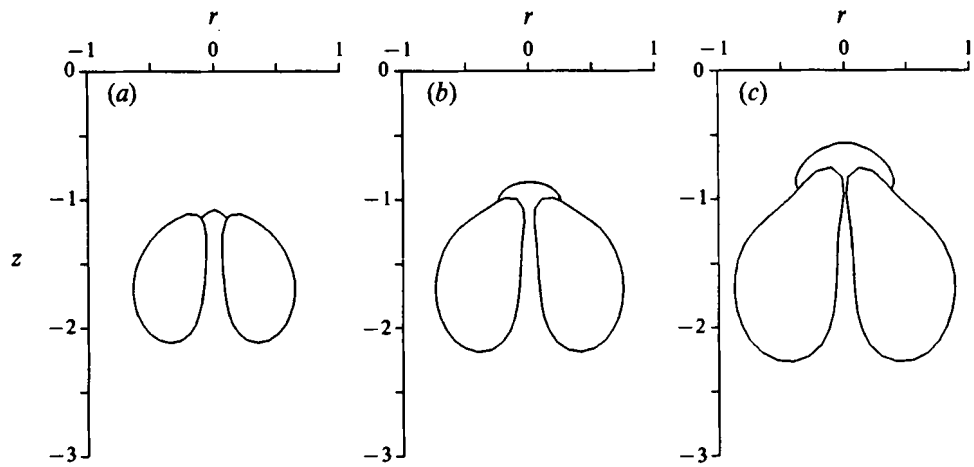

FIGURE 15. The motion of the toroidal bubble that evolves from the collapse and rebound shown in figure 3. The circulation is $\Delta\phi = -2.304$. (*a*) $t = 2.6225$, (*b*) 2.7321, (*c*) 2.9207.

6. Discussion

In this paper we have developed an algorithm for computing the motion of toroidal bubbles. Although sharing some similarities with the method of Lundgren & Mansour (1991), that developed here has particularly addressed the case of the toroidal bubble formed upon the collapse of transient cavities undergoing very large-amplitude oscillations, in contrast to the constant-volume bubbles considered in Lundgren & Mansour's recent investigation. Furthermore, we have here attempted to undertake the calculation from the moment that jet impact occurs, rather than begin the computation in the toroidal geometry by assuming a simplifying bubble shape. The treatment of the vortex ring is also different. Here we have introduced a cut in the flow domain in order that we may consider it as singly connected, whereas Lundgren & Mansour have explicitly added a vortex ring potential to a single-valued potential function, in order to account for the circulation in the flow.

The results presented here have demonstrated the oscillatory nature of toroidal bubbles with rebound observed. The initial depression in the bubble shape due to the flow around the torus gradually vanishes as the flow field evolves and the motion appears to be stable. These results are qualitatively in accord with recent experiments, the results of Vogel *et al.* (1989) showing multiple oscillations of such bubbles. It is only after several oscillations that a wave-like disturbance, travelling around the torus, appears and ultimately leads to the break up of the bubble. Although the analysis of Pedley (1968) is not applicable to the large-amplitude oscillations of toroidal bubbles considered here or in recent experiments, it indicates the finite lifetime of vortex ring bubbles with their breakup caused by surface tension instabilities. The experiments of Vogel *et al.* also suggest that in some cases a permanent vortex ring bubble is formed on the second collapse, despite jet penetration occurring on the first collapse. The results presented here have indicated a mechanism by which this may occur. In some cases the fluid flowing through the torus thins upon re-expansion and presumably then disconnects, resulting in a flow domain that is once again singly connected.

This process by which the toroidal bubble resumes a connected topology may provide a mechanism for the formation of what appear to be very sharp jets

penetrating a large distance beyond the main part of the bubble surface (Vogel *et al.* 1989). We may postulate that upon resuming a singly connected topology, the outflow of fluid caused by re-expansion causes the ejection of the element of fluid that remains penetrating the bubble. This may be the source of the sharp jet. We remark in this context that the surface about the disconnection point is characterized by very high curvatures. Hence we might suppose that the surface tension forces acting on the elements of the fluid about this point are significant and the action of this force will be to eject these elements of fluid from the bubble. This is perhaps a mechanism for the creation of what appear to be sharp jets. We further note that this behaviour is evident in experiments involving bubbles whose maximum radii are of the order of 10^{-3} m, so that the radii of curvature associated with jet formation may be several orders of magnitude less than this.

An initial investigation of this question may be pursued by including surface tension in the model. However, to do so would necessitate an understanding of the role that surface tension plays in the initial impact of the jet upon the far side of the bubble, noting that the jet tip is characterized by a very high curvature. This aspect is an open question and a very difficult one as the mechanism by which the two contacting surfaces breakdown and become one is not well understood. Oguz & Prosperetti (1989) have recently considered this question, but perform calculations of the motion of two surfaces after such a contact by assuming that they are initially connected by an element of fluid. Their work indicates a complex behaviour, with a wave-like disturbance arising from the contact point leading to fluid contact at a number of points away from the initial contact element. The gas entrapped between these multiple contact points presumably forms a collection of bubbles. Furthermore, it has been put forward by Vogel *et al.* (1989) that in some cases the surfaces at contact do not break down and form one, but remain separated by a thin layer of gas, with the impact of the jet pushing the surface of the bubble ahead, the behaviour much as if a jet impacted upon a membrane. Surface tension must play a significant role in preventing the breakdown of the surfaces if this is a feasible behaviour.

For large-scale bubble phenomena such as that caused by an underwater explosion, however, surface tension is not expected to play a major role at any stage of the motion, although in the context of the disconnection of the fluid flowing through the torus, if this fluid becomes sufficiently thin the high temperature of the detonation products or fluctuations in the pressure field may be sufficient to cause this fluid to break up, yielding a singly connected flow domain. Remarking further on the possibility of this disconnection process, an investigation of some relevance is that of Chesters & Hofman (1982) in which the coalescence of two slowly approaching bubbles in a viscous fluid has been considered. The two bubbles are initially separated by a thin film of liquid which must break down for the two bubbles to become one. This is similar to the situation that arises when the fluid flowing through the torus thins and then must break up for the flow field to resume a singly connected topology. The analysis suggests a complex behaviour with the breakup of the surface occurring around some ring encircling the initial point of minimum fluid thickness. It remains for further investigation to clarify the behaviour of surfaces upon contact and breakup in order that the influence of these phenomena on the motion of toroidal bubbles may be determined.

Once a toroidal geometry has been assumed the method described in this paper may be used to compute the motion of the bubble. Furthermore, the ideas developed here may be applied to the transition to a doubly connected flow geometry that occurs when steep surface waves on water overturn.

I would like to thank Professor J. R. Blake for helpful discussions and for commenting on this manuscript, and Dr A. Kucera who provided his boundary integral code, which was modified for this investigation. I would further like to thank two of the referees who provided constructive comments of considerable detail. This work was carried out in the Department of Mathematics, The University of Wollongong, Australia and the School of Mathematics and Statistics, The University of Birmingham, UK.

REFERENCES

BAKER, G. R., MEIRON, D. I. & ORSZAG, S. A. 1980 Vortex simulations of the Rayleigh–Taylor instability. *Phys. Fluids* **23**, 1485–1490.

BAKER, G. R., MEIRON, D. I. & ORSZAG, S. A. 1982 Generalized vortex methods for free-surface flow problems. *J. Fluid Mech.* **123**, 477–501.

BAKER, G. R., MEIRON, D. I. & ORSZAG, S. A. 1984 Boundary integral methods for axisymmetric and three-dimensional Rayleigh–Taylor instability problems. *Physica* **12** D, 19–31.

BATCHELOR, G. K. 1967 *An Introduction to Fluid Dynamics*. Cambridge University Press.

BENJAMIN, T. B. & ELLIS, A. T. 1966 The collapse of cavitation bubbles and the pressures thereby produced against solid boundaries. *Phil. Trans. R. Soc. Lond.* A **260**, 221–240.

BEST, J. P. & KUCERA, A. 1992 A numerical investigation of non-spherical rebounding bubbles. *J. Fluid Mech.* **245**, 137–154.

BLAKE, J. R. & GIBSON, D. C. 1987 Cavitation bubbles near boundaries. *Ann. Rev. Fluid Mech.* **19**, 99–123.

BLAKE, J. R., TAIB, B. B. & DOHERTY, G. 1986 Transient cavities near boundaries. Part 1. Rigid boundary. *J. Fluid Mech.* **170**, 479–497.

BLAKE, J. R., TAIB, B. B. & DOHERTY, G. 1987 Transient cavities near boundaries. Part 2. Free surface. *J. Fluid Mech.* **181**, 197–212.

CHESTERS, A. K. & HOFMAN, G. 1982 Bubble coalescence in pure liquids. *Appl. Sci. Res.* **38**, 353–361.

DEBOOR, C. 1978 *A Practical Guide to Splines*. Springer.

GUERRI, L., LUCCA, G. & PROSPERETTI, A. 1981 A numerical method for the dynamics of non-spherical cavitation bubbles. In *Proc. 2nd Intl Colloq. on Drops and Bubbles*, pp. 175–181. JPL Publication 82–7, Monterey, California.

HOLT, M. 1977 Underwater explosions. *Ann. Rev. Fluid Mech.* **9**, 187–214.

KUCERA, A. 1993 A boundary integral method applied to the growth and collapse of bubbles near a rigid boundary. *J. Comput. Phys.* (submitted).

LAUTERBORN, W. 1982 Cavitation bubble dynamics – new tools for an intricate problem. *Appl. Sci. Res.* **38**, 165–178.

LAUTERBORN, W. & BOLLE, H. 1975 Experimental investigations of cavitation bubble collapse in the neighbourhood of a solid boundary. *J. Fluid Mech.* **72**, 391–399.

LONGUET-HIGGINS, M. S. & COKELET, E. D. 1976 The deformation of steep surface waves on water. I. A numerical method of computation. *Proc. R. Soc. Lond.* A **350**, 1–26.

LUNDGREN, T. S. & MANSOUR, N. N. 1991 Vortex ring bubbles. *J. Fluid Mech.* **224**, 177–196.

OGUZ, H. N. & PROSPERETTI, A. 1989 Surface-tension effects in the contact of liquid surfaces. *J. Fluid Mech.* **203**, 149–171.

OGUZ, H. N. & PROSPERETTI, A. 1990 Bubble entrainment by the impact of drops on liquid surfaces. *J. Fluid Mech.* **219**, 143–180.

PEDLEY, T. J. 1968 The toroidal bubble. *J. Fluid Mech.* **32**, 97–112.

PLESSET, M. S. & CHAPMAN, R. B. 1971 Collapse of an initially spherical vapour cavity in the neighbourhood of a solid boundary. *J. Fluid Mech.* **47**, 283–290.

RAYLEIGH, LORD 1917 On the pressure developed in a liquid during the collapse of a spherical void. *Phil. Mag.* **34**, 94–98.

SEYBERT, A. F., SOENARKO, B., RIZZO, F. J. & SHIPPY, D. J. 1985 An advanced computational method for radiation and scattering of acoustic waves in three dimensions. *J. Acoust. Soc. Am.* **77**, 362–368.

TAIB, B. B. 1985 Boundary integral methods applied to cavitation bubble dynamics. PhD thesis, University of Wollongong, Australia.

VOGEL, A., LAUTERBORN, W. & TIMM, R. 1989 Optical and acoustic investigations of the dynamics of laser-produced cavitation bubbles near a solid boundary. *J. Fluid Mech.* **206**, 299–338.